JOURNAL OF Materials CHEMISTRY

Manipulating core–shell reactivities for processing nanoparticle sizes and shapes

Mathew M. Maye and Chuan-Jian Zhong*

Department of Chemistry, State University of New York at Binghamton, Binghamton, New York, USA 13902. E-mail: cjzhong@binghamton.edu

Received 22nd February 2000, Accepted 8th May 2000
Published on the Web 29th June 2000

This paper describes new findings of an investigation of thermally-activated core–shell reactivities of nanoparticles in solutions for processing size, shape and surface properties. Gold nanoparticles of $\approx$2 nm core sizes with thiolate monolayer encapsulation were chosen as a model system for the manipulation of reaction parameters, including annealing effect, core composition and shell structure. It is revealed that, upon an evolution of particle sizes, annealing treatment of the solution in the presence of encapsulating thiols can lead to the formation of highly monodispersed nanoparticles. New insights into shell desorption, core coalescence and shell re-encapsulation have been provided by dependencies of the evolution temperature on the capping thiolate chain length and the core alloy composition. Transmission electron microscopic, FTIR and UV-Visible techniques were used to characterize the morphological and chemical properties. The implication of the results for the development of abilities in chemical processing core–shell nanoparticles is discussed.

Introduction

Thermally-activated core–shell reactivities have recently been considered as a strategy for inducing size and shape changes of nanoparticles from solutions of preformed thiolate-capped gold nanoparticles.[1] The work described herein reports new findings on manipulating the core–shell reactivities for processing size and shape properties. Gold nanoparticles encapsulated with alkanethiolate monolayers synthesized by Schiffrin's two-phase protocol[2] were studied as a model system. This class of composite nanomaterials is interesting because there are considerable potential technological applications in areas of microelectronics, optical devices, magnetic materials, catalysis and chemical recognition.[3–8] Our investigation of this process is aimed at the development of a processing route for controlling size, shape and surface properties of the nanoparticles, an area with tremendous opportunities for tuning the nanometre-sized building blocks towards constructing interfacial nanomaterials for chemical and biological sensing, catalysis and recognition applications.[3,9–12]

Scheme 1 depicts hypothesized core–shell reactivities of the alkanethiolate-capped gold nanoparticles under thermal activation. Larger core sizes result from an evolution of the smaller-sized starting particles *via* sequential shell desorption, core coalescence and shell re-encapsulation. While two-phase synthesis[2] of the small-sized particles, *e.g.*, $\approx$2 nm core sizes, is relatively easy by using large thiol-to-gold ratios,[2,7] larger-sized nanoparticles can be formed by decreasing the ratio. This type of manipulation is viable for producing different-sized nanoparticles but requires extensive synthetic work and large amounts of reagents. There are a number of other approaches to developing size and shape control abilities, including syntheses carried out at different temperatures[7c] and methods including seeding,[13] templating,[14] using a shape-inducing agent,[15–18] and fractional separation.[19] Fundamentally, however, relatively little is known about the mechanistic aspects for a precise control of shapes and sizes. The concept of heating-induced growth of metal or metal oxide particles is not new (*e.g.*, traditional Ostwald ripening).[20] Such treatments were utilized for systems supported on substrates in processes involving nucleation, dissolution and growth,[21] and in several recent examples involving synthesis and treatments at elevated temperatures.[7c,17b,22] These processes, however, do not involve a direct exploitation of the reactivities at both molecular shells and nanocrystal cores, which we believe may offer new pathways for size and shape manipulation. This is largely in view of the inherently dynamic process due to changes in the chemical potentials of both particles and environmental components.

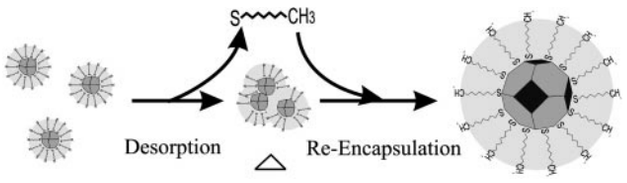

Scheme 1 A schematic illustration of the core–shell reactivities in the thermally-activated size and shape evolution process of thiolate-capped nanoparticles.

Our exploration stems first from recognition of the versatile reactivities at the molecular level. In comparison with conventional colloids and many types of nanoparticles synthesized by reverse micelle, polymer encapsulation and vapor-phase production,[3b] the encapsulation by alkanethiolate monolayers possesses several unique attributes,[3a] including, for example, air stability, reversible solubility in common organic solvents, and molecule-like reactivities involving both end-group functionalization and core–shell binding. Examples have been abundantly demonstrated for solutions of organized or highly-dispersed particles.[23] The possibilities of various core–shell structural combinations are thus expected to manipulate the interfacial chemical potentials, and ultimately to facilitate re-sizing and re-shaping reactivities. In this report, we describe intriguing findings of an investigation of these manipulation factors. In addition to the effect of solution annealing on particle size and shape monodispersity, effects of the core compositions and the shell structures are investigated to understand the structure–reactivity relationship governing the thermally-activated chemical processes for size and shape controls.

Experimental

Chemicals

The thiols used were butanethiol (BT, 99+%), decanethiol (DT, 96%), dodecanethiol (DDT, 98+%), and hexadecanethiol (HDT, 98.5+%). The precursor metal compounds were hydrogen tetracholoroaurate ($HAuCl_4$, 99%), silver nitrate (99%), potassium hexachloroplatinum(IV) (K_2PtCl_6, Baker & Company Inc.). Other chemicals included tetraoctylammonium bromide (TOABr, 99%). sodium borohydride (99%), toluene (99.8%), hexane (99.9%), and potassium bromide (99+%). All chemicals were purchased from Aldrich and used as received, unless otherwise noted. Water was purified with a Millipore Milli-Q water system.

Synthesis

Gold nanoparticles of $\approx$2 nm core size encapsulated with alkanethiolate monolayer shells were synthesized by Schiffrin's two-phase protocol.[2,7c] Briefly, $AuCl_4^-$ was first transferred from aqueous $HAuCl_4$ solution (10 mM) to toluene solution by phase transfer reagent TOABr (36 mM). Thiols, *e.g.*, DT, were then added to the solution (21 mM) at a DT : Au mole ratio of 2 : 1. An excess (12 $\times$) of aqueous reducing agent ($NaBH_4$) was slowly added into the solution. The reaction was allowed proceed under stirring at room temperature for 4 hours, producing a dark-brown solution of DT-encapsulated nanoparticles. The solution was subjected to solvent removal in a rotary evaporator at room temperature followed by multiple cleaning procedures using ethanol to purify the 2 nm sized particles.

The synthesis of gold alloy nanoparticles of an average core size $\approx$3.5 nm, Au–Ag and Au–Pt, followed the procedures reported recently.[7b] The Au–Ag nanoparticles were synthesized with DT encapsulation, whereas the Au–Pt was synthesized with DDT encapsulation. Briefly, the Au–Ag particles were synthesized in a 1 : 4 feeding ratio of $HAuCl_4$ to $AgNO_3$ dissolved in 25 mL of water. This solution was then added to a toluene solution of TOA^+ similar to the synthesis of gold nanoparticles. DT was then added to this solution followed by adding $NaBH_4$ (dropwise), resulting in a dark brownish solution containing the Au–Ag alloy nanoparticles. Au–Pt nanoparticles were synthesized in a similar manner but using a 1 : 1 ratio of $HAuCl_4$ to $K_2Pt_2Cl_6$, and DDT encapsulating thiol. The resulting nanoparticle solution appeared black.

Heat treatment

The heat treatment provides the thermal activation of the core–shell reactivities, which was performed with solutions of pre-synthesized gold or alloy nanoparticles in a temperature range of 25 to 180 °C. The solution of nanoparticles directly resulting from the synthesis was initially pre-concentrated by a factor of 15–20 in molar concentration before a subsequent heating to higher temperatures. During the entire heating process, the silicone oil bath was maintained at a constant temperature between 150–190 °C that was higher than the sample temperature depending on the chemical compositions of the core–shell nanoparticle systems. The temperatures both in the oil bath and the sample were measured either using a thermometer or a thermocouple probe, details of which were reported recently.[1a]

In the "solution annealing" treatment, the above nanoparticle solution was first heated to the evolution temperature, as judged by color change of the solution or by UV-Vis monitoring of the surface plasmon resonance band. The solution was then mixed with a small volume of toluene solution containing encapsulating thiols ($\approx$100 mM). The solution was quickly brought from the evolution temperature to (or slightly below) the boiling point of toluene (110 °C), and was then allowed to anneal at a lower temperature, 80–100 °C, for a certain time duration, typically several hours.

Instrumentation

Fourier transform infrared spectra were acquired with a Nicolet 760 ESP FTIR spectrometer that was purged with boil-off from liquid N_2. The spectrometer was equipped with a liquid nitrogen-cooled HgCdTe detector. The nanoparticle sample was ground with KBr into fine powders, and pressed into a pellet at 15000 psi. The IR spectra were collected over the range of 400–4000 cm^{-1}. UV-Visible (UV-Vis) spectra were acquired with a HP8453 spectrophotometer. Nanoparticle samples were dissolved in hexane. The spectra were collected over the range of 200–1100 nm. Transmission electron microscopy (TEM) was performed on Hitachi H-7000 electron microscope (100 kV). The nanoparticle samples dissolved in hexane or toluene solution were drop cast onto a carbon-coated copper grid sample holder followed by natural evaporation at room temperature.

Results and discussion

1. The effect of annealing on the evolved size and shape

The "solution annealing" refers to a treatment procedure by which the temperature of the solution, upon the observation of a solution color change at the evolution temperature, was lowered to $\approx$100 °C and maintained for a certain time duration. An additional solution of encapsulating thiols ($\approx$100 mM) was also added to the solution to ensure re-encapsulation during annealing. Such an annealing treatment was found to affect the size and shape homogeneity of the resulting nanoparticles with remarkable effectiveness. Fig. 1 shows a representative TEM image of the DT-capped Au nanoparticles evolved from such annealing treatment. The image of the precursor 2 nm particles is inserted for comparison. Clearly, the evolved nanoparticles show dramatic changes in size, shape and homogeneity in comparison with the precursor nanoparticles, due to a combination of the initial heating-induced evolution and the subsequent annealing produced re-shaping or re-sizing effects.

Several morphological changes are evident from observations of the solution annealing process. First, the size distribution is strikingly narrow, as shown in Fig. 2 by the contrast of the size distribution histograms for both nanoparticles. The 2 nm particle core sizes were 1.9 $\pm$ 0.7 nm, which is consistent with data reported recently.[7c] The particle shapes

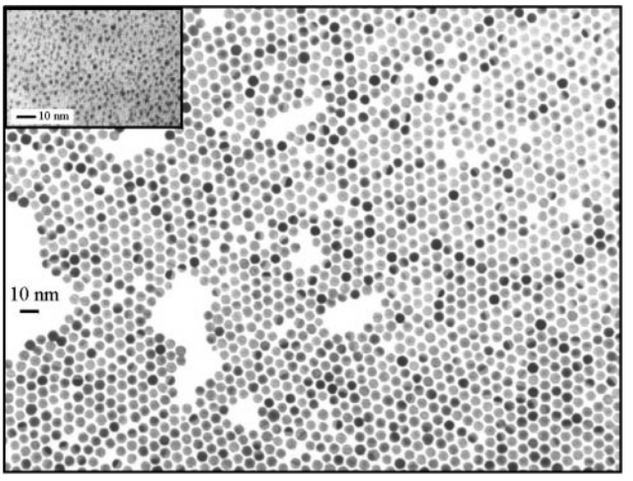

Fig. 1 TEM micrographs of DT-encapsulated Au nanoparticles prepared by the solution annealing process in the presence of excess DT following the thermally-activated size evolution. The insert shows the TEM image of the precursor nanoparticles.

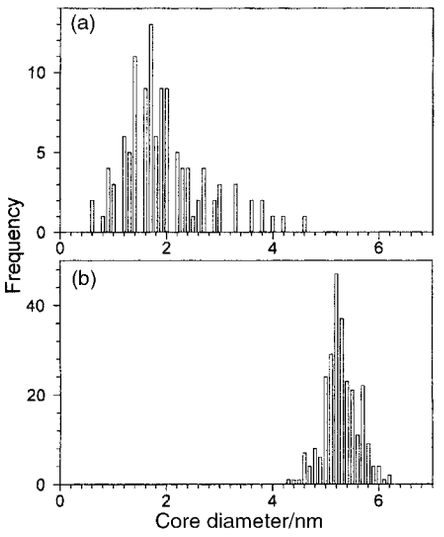

Fig. 2 Histograms of the nanocrystal core sizes comparing the precursor (a) and the evolved product (b). The data were determined from the TEM image of Fig. 1 (particle count: 130 (a), 260 (b)).

appear as non-uniform polyhedrons. In sharp contrast, the data for the evolved nanoparticles display increased core size with a very narrow size distribution, *i.e.*, 5.3 ± 0.3 nm, much narrower than the 2 nm starting particles.

Secondly, a close examination of the particle shapes reveals a predominant presence of faceted particles with a significant percentage that seem to exhibit "hexagon" outlines. Particularly intriguing is the presence of two types of particle morphologies as reflected by the darkness of the particles in the TEM image. While most particles display plate-like features as hinted by the uniform gray color across the particle, a number of particles exhibit a "3D" morphology as reflected by the distinctive darkness of the particles. On the basis of the particle cross-section views shown in the image of Fig. 1, the percentage of the dark particles is roughly 25%. While not completely clear about the origin, we believe that such a difference is suggestive of the presence of two types of shape outline.

Thirdly, the uniform spacing between the nanoparticles with a predominant hexagonal packing array feature is remarkable. Edge-to-edge distances are estimated to range from 0.7 to 1.4 nm with an average distance of ≈ 1.0 nm. This value corresponds closely to the distance expected for an interdigitation of alkyl chains between shells of the neighboring nanoparticles.[24]

In comparison with recent data showing size and shape evolution of nanoparticles upon heat treatment,[1] the above annealing-produced morphological features constitute clear evidence for the existence of a further re-sizing and re-shaping effect for the evolved particles in the annealing process. While the mechanistic details remain to be investigated, two cooperative processes are believed to be responsible for the experimental observation. The first involves thermally-driven desorption of the shell components followed by coalescence of the nanoparticle cores. The second involves the re-shaping or re-sizing that minimizes the chemical potentials followed by competitive re-encapsulation of thiolate shells under the annealing conditions. The latter is an analogy to thermal annealing of solid samples. The key distinction is the involvement of a series of chemical processes such as thiolate encapsulation, desorption and re-encapsulation, during which the nanocrystal facets and corners are further developed into energetically-more favorable states. Based on these qualitative considerations, we expect that manipulations of the core composition, shell structures and solution components should have profound impacts on the evolution reactivities and interfacial energies of the thermally-activated core–shell nanoparticles, which are discussed next.

2. Chemical manipulation of core–shell reactivities in the thermal evolution

The effects of two types of structural manipulations, *i.e.*, chain length of the thiolate shell and composition of the nanocrystal core, on the core–shell reactivities in the size and shape evolutions are investigated. To gain insights into these effects, three different types of sample systems were studied, each with varied characteristics in the core–shell structure or composition. The first type involved Au nanoparticles with the difference in chain length for the encapsulating thiolates, including BT, DT and HDT. The second type involved samples capped with thiolates of one chain length in the presence of thiols of another chain length. The third type involved gold alloy nanoparticles, gold–silver (Au–Ag) and gold–platinum (Au–Pt).

The thermally-activated evolution in particle sizes for these samples is shown by a set of representative TEM images. Fig. 3 shows the result of a Au nanoparticle system with HDT thiolates encapsulation, whereas Fig. 4 displays the results of two alloy nanoparticle systems, Au–Ag (A) and Au–Pt (B). These samples were collected from the heating solutions upon indication of the size evolution without an extensive annealing treatment. Clearly, all samples showed the size evolution to a core size range of ≈ 5–7 nm. Domains of hexagon-type packing for one-layer nanoparticles can be identified for each sample, though the domain sizes vary from sample to sample. The feature is consistent with those previously reported for DT-capped nanoparticles.[1a] Interestingly, a long-range ordering with a stripe-like array feature can also be observed in a two-layer domain for the Au nanoparticles capped with long-chain thiolates (HDT) (Fig. 3). Based on the elongated dimension feature of the particles in the array (*i.e.*, 5.3 nm long and 3.8 nm wide), we believe that the second layer adopted a slight offset registration with respect to the first layer. Other types of registration were previously reported for nanoparticles capped with DT and other shells.[1a,6] For the alloy nanoparticles, the average core size of the evolved nanoparticles was in the 5–

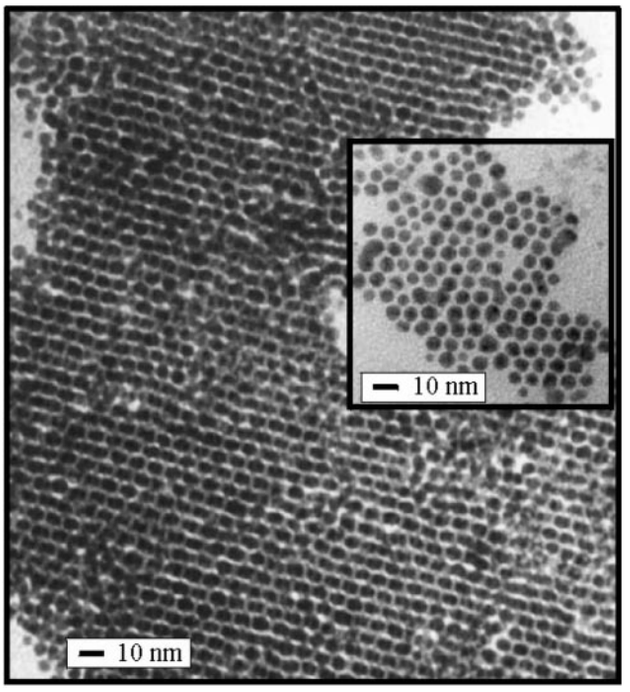

Fig. 3 TEM micrographs of the nanoparticle product in two domains: two-layer and one-layer (insert). The product was evolved from HDT-encapsulated Au nanoparticles.

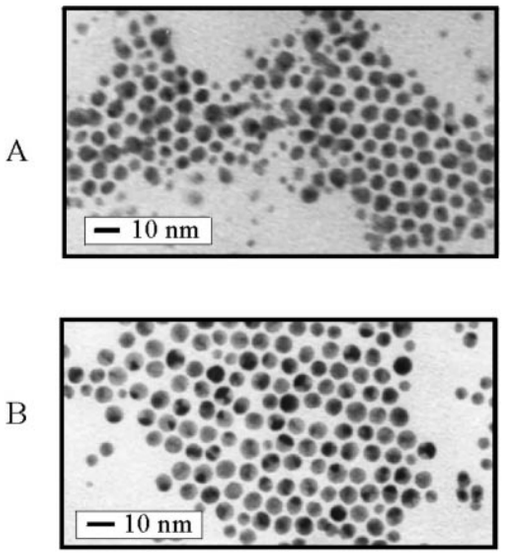

Fig. 4 TEM micrographs of the products evolved from DDT-capped Au–Ag (A) and DT-capped Au–Pt (B) nanoparticles

6 nm range. A small percentage of smaller core sizes were also evident. The origin could be due to the lack of annealing as described earlier or due to other possible effects involving two different core compositions, which are under further investigation. Further insights are provided by studies of effects of both chain–chain interaction of capping thiolates and core–core interaction of alloy particles.

Effect of the thiolate shell structures. To demonstrate the structural effect of the chain length of the capping alkanethiolates, we report mainly the results from three chain length systems including BT, DT and HDT. The basis for the assessment of the chain length effect on the observed evolution temperatures and structural properties of the resulting nanoparticles is the difference in binding energies of alkanethiolates to the particle. While Au–S bonding is identical for the three chain lengths, the contribution of a cohesive energy due to chain–chain interactions determines the overall binding strength. As a result, the thermal stability and the core–shell reactivities for the encapsulation and re-encapsulation should be manipulated by varying the chain length.

Fig. 5 shows a set of UV-Vis data comparing the Au–BT, Au–DT and Au–HDT nanoparticles before and after the heating-induced evolution. The optical absorption band is originated from the surface plasmon (SP) resonance of the nanoparticles.[7c,25] Except for the Au–BT system which formed an insoluble product, both Au–DT and Au–HDT showed a similar increase of the SP band at 520 nm, which is consistent with the evolution of the particle sizes as revealed by the TEM data (Fig. 1 and 3). The spectrum for the evolved Au–BT sample was taken in between the observation of the initial evolution product and the observation of the eventual formation of the insoluble product. It reveals a small hint of the SP band resulting from a small fraction of the particles that were soluble. The dependence of the evolution processes on the chain length of the encapsulating thiolates is reflected by the different values of the evolution temperature and the associated time length, as summarized in Table 1.

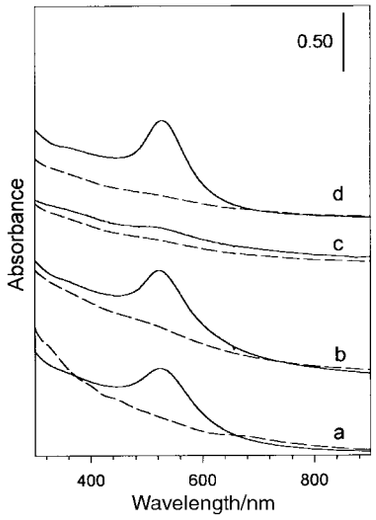

Fig. 5 UV-Visible spectra comparing the Au nanoparticle samples before (dashed lines) and after (solid lines) the thermally-activated size and shape evolution. (a) HDT-capped Au, (b), DT-capped Au, (c) BT-capped Au, (d) BT-capped Au evolved in the presence of HDT.

The evolution temperature can be defined as the temperature at which there is a color change or an increase of the SP band as shown in Fig. 5 for the heated nanoparticle samples. This temperature was found to increase with increasing chain length of the shell thiolates. The length of time needed for the evolution (t_E) to occur at a constant bath temperature was also shown to increase with the chain length. For example, the evolution temperature of the DT-capped Au occurred at $\approx$138 °C after heating for 45 minutes at a bath temperature of 150–160 °C. The product was soluble in toluene with a deep red color distinctively different from the dark brown starting particles. Importantly, a comparison of the data for the nanoparticles capped with shorter or longer capping thiolate chain length reveals remarkable differences in both temperature and length of time needed. For example, Au capped with BT showed a color change at $\approx$125 °C upon heating for about 30 minutes. This change was however quickly followed by the formation of an insoluble product. In contrast, nanoparticles capped with HDT exhibited the color change to a deep red at $\approx$155 °C after about 60 min of heating in the same oil bath. Clearly, the evolution temperature and the time increase with increasing chain length of the capping alkanethiolates (Table 1). In other words, a higher temperature is required for the evolution of nanoparticles capped with thiolates of longer chain structures than those with shorter chain thiolates. It is important to note that the t_E values reported do not provide any kinetic assessment on the evolution, rather an assessment of energy needed to achieve the evolution temperature.

These results are qualitatively consistent with both an energetic consideration and experimental thermochemical data reported for the core–shell nanoparticle systems. Energetically, more energy is needed to desorb the thiolates before the core–core coalescence can occur. Consider, for example, the cohesive energy of the alkanethiolate shells on Au. It is well known that for monolayer assembly on gold surfaces, thiolate chains are interdigitated *via* a van der Waals interaction. Such a

Table 1 A comparison of the evolution temperature (T_E) and the approximate time (t_E) taken to reach T_E for the thermally-activated evolution of different core–shell nanoparticle samples

	Thermally-activated evolution	
Sample[a]	T_E/°C	t_E/min
Au/BT	125	30
Au/DT	138	45
Au/HDT	155	60
Au/BT→Au/HDT	130	30
Au/Ag(1 : 4)/DT	155	60
Au/Pt(1 : 1)/DDT	165	50

[a]Au/BT stands for an Au nanoparticle encapsulated within a BT monolayer; Au/BT→Au/BT represents the change of encapsulation *via* heating Au/BT in the presence of HDT.

cohesive energy is estimated to be about 1.0 kJ mol^{-1} per (CH_2) group.[26] This consideration qualitatively suggests that the desorption energy increases with increasing chain length of the capping thiolates. Recent differential scanning calorimetry data obtained for Au nanoparticle systems with thiolate encapsulation of different chain lengths have indeed shown that the order–disorder transition temperature increases with increasing chain length,[7c,24,27] consistent with the melting of crystalline alkane hydrocarbons. Our data are thus strong evidence that the chemical reactions involve thermally-activated thiolate desorption in the encapsulating shell.

Re-encapsulation of the evolved nanocrystal cores constitutes another part of the chemical reactivities, which is essential to protect the coalescing particles from forming uncontrollable large aggregates. DT and HDT are clearly effective in this regard, as demonstrated by well-defined sizes and shapes of the resulting particles. In contrast, the formation of insoluble products from heating the nanoparticles capped with BT is suggestive of an ineffective re-encapsulation by the shorter chain length at the evolution temperature. As a result, the coalescing particle cores further aggregate into insoluble larger particles. In view of the demonstrated importance of the shell encapsulation, we envision that the manipulation of the solution thiol composition should directly affect the re-encapsulation process. This is demonstrated next by an experiment involving heating the nanoparticles capped with shorter chain thiolates in the presence of thiols of long chain length.

Starting with Au nanoparticles capped with BT, the solution was first heated to the evolution temperature and followed by an addition of a small aliquot of a toluene solution of HDT. Upon further heating, the solution showed a clear color change towards deep red and a soluble product formed. Importantly, as opposed to the formation of insoluble product in the absence of the HDT component, the product in the presence of the HDT was now soluble in the heated solution up to $\approx$180 °C. The temperature for Au/BT→Au/HDT was in fact close to the evolution temperature for the nanoparticles capped with HDT as described earlier (Table 1). The UV-Vis data for the evolution of the BT-capped Au in the HDT-containing solution are included in Fig. 5. In comparison with data for the evolution products for Au–DT and Au–HDT nanoparticles, the SP band for the Au–BT product is now comparable. The greater affinity of the long chain HDT towards gold than that of BT is responsible for the re-encapsulation, ensuring that the resulting particles were not subject to a further aggregation. The role of solution thiol composition for the eventual re-encapsulation is similar to the recent finding on the importance of the highly hydrophobic and polar TOA^+ species in the size and shape evolutions.[1a] The combined results demonstrate that the thermally-activated evolution indeed involves a series of core–shell reactivities, including the initial desorption of the shell, the coalescence of the gold clusters into larger particles, and the eventual re-encapsulation of the particles, as has been schematically illustrated in Scheme 1.

FTIR characterizations probing the capping shell structures of the evolved products provided further structural evidence for the re-encapsulation of thiolate shell structures, as shown by a representative set of FTIR spectra in Fig. 6. The C–H stretching bands are listed in Table 2. First, the overall spectral features for the alkanethiolate encapsulation remain unchanged before and after the evolution, demonstrating the structural integrity. Secondly, a shift of the methylene stretching bands to lower energy by $\approx$2–6 cm^{-1} is observed for the evolved particles, indicative of a more crystalline packing structure of the alkanethiolates. The results are consistent with previous data on larger-sized nanoclusters.[28] And lastly, the re-encapsulation by HDT for heating Au/BT in the presence of HDT (*i.e.*, Au/BT→Au/HDT) is confirmed by the detection of C–H bands diagnostic of HDT thiolates.

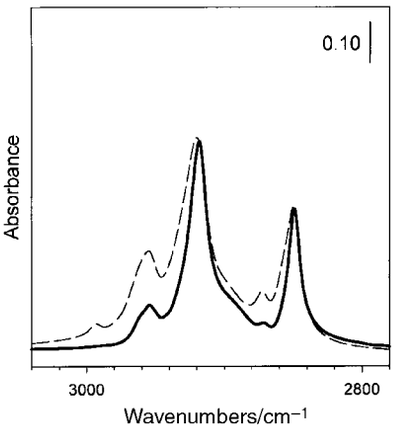

Fig. 6 FTIR spectra of powder samples in KBr pellets for the product evolved from the HDT-encapsulated Au nanoparticles. The C–H stretching region for the asymmetric and symmetric stretching bands of methylene and methyl groups is shown.

Effect of the nanoparticle core composition. Considering differences of surface atomic distribution of nanoparticle cores for thiolate binding and crystal growth during the core–shell reactions or processes, we have examined several nanoparticle systems with alloy core compositions.[7b]. Fig. 7 shows a set of UV-Vis data for two types of alloy gold nanoparticles, *i.e.*, Au–Ag and Au–Pt. For Au–Pt particles, the initial average core size was about 2 nm. Like 2 nm Au particles, no pronounced SP band was observed at the 520 nm wavelength range in initial dark brown Au–Pt solution, though a large band was observed at $\approx$280 nm related to the Pt-component.[29] Upon heating the solution to a temperature of 175 °C, the particle solution turned red and the UV-Vis spectrum displayed a band at 520 nm similar to that for the 5 nm Au nanoparticles. The result is indicative of a size change for the evolved particles, as confirmed by TEM data (Fig. 4B). Clearly, the presence of a Pt component in the core did not prevent the particles from core–core coalescence, growth and encapsulation with thiolate shells. FTIR data (Table 2) in the region of the C–H stretching bands are supportive of the re-encapsulation of the evolved particles by DT shell.

Interestingly, the result for Au–Ag nanoparticles is distinctively different from the above observation. The UV-Vis data showed however subtle color and spectral changes depending on the heating conditions. For the initial Au–Ag particles (average core size $\approx$3.5 nm), the SP band was displayed at 462 nm. In addition to displaying an enhancement of the SP band, the evolved particles showed two types of SP band shift, *i.e.*, blue and red shifts. The blue shift (from 462 to 451 nm) was observed for the initial evolution, *i.e.*, samples taken after 5–10 minutes upon heating to 130–140 °C. The red shift (from 451 to 475 nm) was observed for samples taken after further heating the nanoparticle solution to a temperature of $\approx$160 °C. The resulting nanoparticle products were soluble in toluene solution, even for samples taken after heating to $\approx$190 °C. The overall SP band enhancement is consistent with the size evolution into 5–6 nm core sizes as revealed by the TEM data (Figure 4A). Again, the re-encapsulation of the evolved nanoparticles by DT shell is confirmed by FTIR data (Table 2), which showed the C–H stretching bands comparable to data for the other nanoparticle systems with the same shell encapsulation.

Another interesting characteristic of the evolution for the Au–Ag alloy particles was reflected by the specularly-reflective color of the product in the solid state. For example, upon cleaning and drying the evolved nanoparticle product, the particles displayed a reflective greenish color, which was distinctively different from the black or dark gray colors of the other evolved nanoparticles. This characteristic, while not fully

Table 2 Mode assignments and comparisons of the FTIR bands (cm^{-1}) in the C–H stretching region for KBr-samples of the nanoparticles before and after the thermally-activated evolution

	Before evolution				After evolution			
Sample[a]	$\nu_a(CH_2)$	$\nu_s(CH_2)$	$\nu_a(CH_3)$	$\nu_s(CH_3)$	$\nu_a(CH_2)$	$\nu_s(CH_2)$	$\nu_a(CH_3)$	$\nu_s(CH_3)$
Au/BU	2926	2850	2955	2872	2926	[b]	2955	2870
Au/DT	2920	2850	2955	2872	2917	2848	2956	2965
Au/HDT	2920	2849	2955	2872	2918	2848	2954	2870
Au/Ag/DT	2920	2850	2955	2872	2919	2847	2955	2872
Au/Pt/DDT	2923	2853	2955	2872	2917	2849	2955	2872
Au/BT→Au/HDT	2922	2850	2955	2873		2848	2954	2869

[a]The sample notations are the same as those in Table 1. [b]Not detected.

understood, is believed to reflect a combination effect of both the increased size and the surface re-distribution of Au and Ag components at the nanocrystal core. The reflective feature is likely associated with a predominant segregation of the silver component surrounding the crystal core. The shell encapsulation of the evolved particles was also confirmed by FTIR data (Table 2).

While the above data demonstrate that the thermally-activated size evolution is operative for alloy core composition, an important question is how the relative distribution of the two components evolve around the nanocrystal core surface, which is important for the catalytic applications of the nanomaterials. It was recently demonstrated[7b] that the two components in Ag–Au alloy cluster core are partly segregated. Whether such a segregation is further developed into full segregation as a result of the thermally-activated core–shell reactivities is a subject of our further investigations.[30]

Overall, the results, together with our previous results,[1] have shown that the thermally-activated core–shell based evolution is dependent on core composition, shell structure, annealing temperature, and precursor concentration. These dependencies are cooperative, and may not be treated individually for a kinetic assessment. For example, we may expect that the growth rate follows a second-order kinetic behavior in terms of concentration effect. Experimentally, however, the evolution temperature was also changed upon changing concentration. The evolution temperature was observed at 140 °C for a solution of 12 mM particle concentration, whereas a solution of 1 mM showed an evolution temperature of 120 °C. By further lowering concentration the temperature stayed close to the solvent boiling point and no particle evolution was evident. The observation is associated with the fact that boiling point rises with increasing mole fraction of the nanoparticles.[1] A further complication to the kinetic assessment is due to the change of melting point of particles as a function of core size that increases during the evolution.[1] A detailed understanding of their correlation is needed for a kinetic assessment of the particle growth involving adsorption, coalescence and re-encapsulation processes.

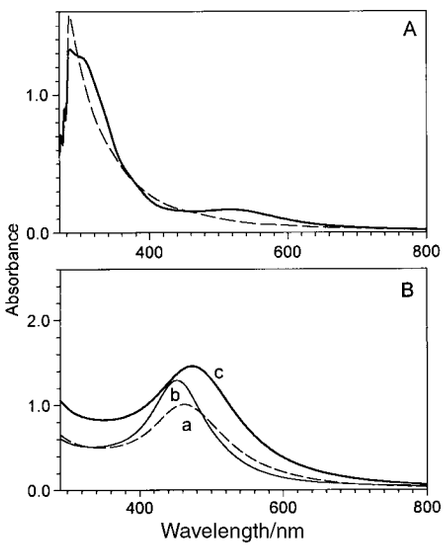

Fig. 7 UV-Visible spectra comparing the alloy nanoparticle samples before (dashed lines) and after (solid lines) the thermally-activated size and shape evolution. (A) DDT-capped Au–Pt. (B) DT-capped Au–Ag. For B, curve b is for the sample taken upon the initial heating treatment and curve c is for the eventual product.

Conclusions

In conclusion, we have demonstrated that structural manipulation of the thiolate-capped nanoparticles in the thermally-activated core–shell reactivities serves as a viable processing route for producing controlled particle sizes and shapes. The size monodispersity of the evolved particles is substantially enhanced by the solution annealing process. Experimental data of TEM, FTIR and UV-Vis have indicated that the chemical reactivities in the evolution process involve shell desorption, core-coalescence and re-encapsulation. The temperature at which the particles change sizes or shapes was found to be dependent on the chain length of the encapsulating thiolates and the compositions of the nanocrystal cores, both of which play important roles in the size and shape evolution. The dependencies of the evolution temperature on the capping thiolate chain length and the core alloy composition have provided new evidence that the thiolate shell desorption and re-encapsulation are two of the critical processes for the control of the core–shell reactivities. Such a control is critical for developing abilities in chemical processing of core–shell nanoparticles for potential catalytic and molecular recognition applications.

Acknowledgements

We thank H. Eichelburger for his expert assistance in the TEM measurement, and W. Zheng for her help in initial work. Acknowledgment is made to the Petroleum Research Fund of the American Chemical Society for partial support of this research. MMM acknowledges the Materials Research Society for support through an UMRI award.

References

1 (*a*) M. M. Maye, W. X. Zheng, F. L. Leibowitz, N. K. Ly and C. J. Zhong, *Langmuir*, 2000, **16**, 490; (*b*) C. J. Zhong, W. X. Zheng, F. L. Leibowitz and H. H. Eichelberger, *Chem. Commun.*, 1999, **13**, 1211.

2 (*a*) M. Brust, M. Walker, D. Bethell, D. J. Schiffrin and R. Whyman, *J. Chem. Soc., Chem. Commun.*, 1994, 801; (*b*) M. Brust, J. Fink, D. Bethell, D. J. Schiffrin and C. J. Kiely, *J. Chem. Soc., Chem. Commun.*, 1995, 1655.

3 (*a*) A. C. Templeton, W. P. Wuelfing and R. W. Murray, *Acc. Chem. Res.*, 2000, **33**, 27 and references therein; (*b*) R. P. Andres, S. Datta, D. B. Janes, C. P. Kubiak and R. Reifenberger in

Handbook of Nanostructured Materials and Nanotechnology, vol. 3, Academic Press, San Diego, 2000, p. 179, and references therein.
4 C. J. Kiely, J. Fink, M. Brust, D. Bethell and D. J. Schiffrin, *Nature*, 1998, **396**, 444.
5 G. Schon and U. Simon, *Colloid Polym. Sci.*, 1995, **273**, 101; G. Schon and U. Simon, *Colloid Polym. Sci.*, 1995, **273**, 202.
6 (*a*) J. Fink, C. J. Kiely, D. Bethell and D. J. Schiffrin, *Chem. Mater.*, 1998, **10**, 922; (*b*) D. Bethell, M. Brust, D. J. Schiffrin and C. J. Kiely, *J. Electroanal. Chem.*, 1996, **409**, 137; (*c*) M. Brust, D. Bethell, D. J. Schiffrin and C. J. Kiely, *Adv. Mater.*, 1995, **7**, 795.
7 (*a*) R. H. Terrill, T. A. Postlethwaite, C. H. Chen, C. D. Poon, A. Terzis, A. Chen, J. E. Hutchison, M. R. Clark, G. Wignall, J. D. Londono, R. Superfine, M. Falvo, C. S. Johnson, E. T. Samulski and R. W. Murray, *J. Am. Chem. Soc.*, 1995, **117**, 12537; (*b*) M. J. Hostetler, C. J. Zhong, B. K. H. Yen, J. Anderegg, S. M. Gross, N. D. Evans, M. D. Porter and R. W. Murray, *J. Am. Chem. Soc.*, 1998, **120**, 9396; (*c*) M. J. Hoetetler, J. E. Wingate, C. J. Zhong, J. E. Harris, R. W. Vachet, M. R. Clark, J. D. Londono, S. J. Green, J. J. Stokes, G. D. Wignall, G. L. Glish, M. D. Porter, N. D. Evans and R. W. Murray, *Langmuir*, 1998, **14**, 17.
8 (*a*) C. S. Weisbecker, M. V. Merritt and G. M. Whitesides, *Langmuir*, 1996, **12**, 3763; (*b*) S. R. Johnson, S. D. Evans, S. W. Mahon and A. Ulman, *Langmuir*, 1997, **13**, 51.
9 (*a*) M. D. Musick, D. J. Pena, S. L. Botsko, T. M. McEvoy, J. N. Richardson and M. J. Natan, *Langmuir*, 1999, **15**, 844; (*b*) L. A. Lyon, M. D. Musick and M. J. Natan, *Anal. Chem.*, 1998, **70**, 5177.
10 (*a*) C. A. Mirkin, R. L. Letsinger, R. C. Mucic and J. J. Storhoff, *Nature*, 1996, **382**, 607; (*b*) R. Elghanian, J. J. Storhoff, R. C. Mucic, R. L. Letsinger and C. A. Mirkin, *Science*, 1997, **277**, 1078.
11 G. Bauer, F. Pittner and Th. Schalkhammer, *Microchim. Acta*, 1999, **131**, 107.
12 (*a*) F. L. Leibowitz, W. X. Zheng, M. M. Maye and M. M. C. J. Zhong, *Anal. Chem*, 1999, **71**, 5076; (*b*) C. J. Zhong, W. X. Zheng and F. L. Leibowitz, *Electrochem. Commun.*, 1999, **1**, 72; (*c*) W. X. Zheng, M. M. Maye, F. L. Leibowitz and C. J. Zhong, *Analyst*, 2000, **125**, 17.
13 C. D. Keating, M. D. Musick, L. A. Lyon, K. R. Brown, B. E. Baker, D. J. Pena, D. L. Feldheim, T. E. Mallouk and M. J. Natan, *ACS Symp. Ser.*, 1997, **679**, 7.
14 (*a*) P. Ugo, L. M. Moretto, S. Bellomi, V. P. Menon and C. R. Martin, *Anal. Chem.*, 1996, **68**, 4160; (*b*) J. C. Hulteen, C. J. Patrissi, D. L. Miner, E. R. Crosthwait, E. B. Oberhauser and C. R. Martin, *J. Phys. Chem. B.*, 1997, **101**, 7727.
15 (*a*) T. S. Ahmadi, Z. L. Wang, T. C. Green, A. Henglein and M. A. El-Sayed, *Science*, 1996, **272**, 1924; (*b*) Z. L. Wang, J. M. Petroski, T. C. Green and M. A. El-Sayed, *J. Phys. Chem. B.*, 1998, **102**, 6145.
16 M. B. Mohamed, K. Z. Ismail, S. Link and M. A. El-Sayed, *J. Phys. Chem. B*, 1998, **102**, 9370.
17 (*a*) Y.-Y. Yu, S.-S. Chang, C.-L. Lee and C. R. C. Wang, *J. Phys. Chem. B.*, 1997, **101**, 6661; (*b*) M. B. Mohamed, Z. L. Wang and M. A. El-Sayed, *J. Phys. Chem., A*, 1999, **103**, 10255.
18 Y. Zhou, C. Y. Wang, Y. R. Zhu and Z. Y. Chen, *Chem Mater.*, 1999, **11**, 2310.
19 R. L. Whetten, J. T. Khoury, M. M. Alvarez, S. Murthy, L. Vezmar, Z. L. Wang, P. W. Stephens, C. L. Cleveland, W. D. Luedtke and U. Landman, *Adv. Mater.*, 1996, **8**, 428.
20 A. Stella, P. Cheyssac and R. Kofman in *Science and Technology of Thin Films*, Ed. F. C. Matacotta and G. Ottaviani, World Scientific, Singapore, Vol. 57, 1996, p 57.
21 (*a*) M. Miki-Yoshida, S. Tehuacanero and M. Jose-Yacaman, *Surf. Sci.*, 1992, **274**, 569; (*b*) S. Lijima and P. M. Ajayan, *J. Appl. Phys.*, 1991, **70**, 5138; (*c*) L. L. Lewis, J. Pablo and J.-L. Barrat, *Phys. Rev. B.*, 1997, **56**, 2248; (*d*) E. Bart, A. Meltsin and D. J. Huppert, *Phys. Chem.*, 1994, **98**, 10819; (*e*) M. Jose-Yacaman and M. Miki-Toshida, *Phys. Rev.*, 1992, **46**, 1198; (*f*) D. J. Duff, A. C. Curtis, P. Edwards, D. A. Jefferson, F. G. Johnson, A. I. Kirkland and D. E. Logan, *Angew. Chem., Int. Ed. Engl.*, 1987, **26**, 7.
22 (*a*) R. Seshadri, G. N. Subbanna, V. Vijayakrishnan, G. U. Kulkarni, G. Ananthan-krishna and C. N. R. Rao, *J. Phys. Chem.*, 1995, **99**, 5639; (*b*) M. H. Magnusson, K. Deppert, J.-O. Malm, J.-O. Bovin and L. Samuelson, *J. Nanoparticle Res.*, 1999, **1**, 243; (*c*) D. Vollath and D. V. Szabo, *J. Nanoparticle Res.*, 1999, **1**, 235.
23 M. J. Hostetler, A. C. Templeton and R. W. Murray, *Langmuir*, 1999, **15**, 3782.
24 M. J. Hostetler and R. W. Murray, *Curr. Opin. Colloid Interface Sci.*, 1997, **2**, 42 and references therein.
25 M. M. Alvarez, J. T. Khoury, T. G. Schaaff, M. N. Shafigullin, I. Vezmar and R. L. Whetten, *J. Phys. Chem. B*, 1997, **101**, 3706.
26 (*a*) R. G. Nuzzo, L. H. Dubois and D. L. Allara, *J. Am. Chem. Soc.*, 1990, **112**, 558; (*b*) C. J. Zhong and M. D. Porter, *J. Electroanal Chem.*, 1997, **425**, 147.
27 A. Badia, L. Cuccia, L. Demers, F. Morin L.; and R. B. Lennox, *J. Am. Chem. Soc.*, 1997, **119**, 2682.
28 M. J. Hostetler, J. J. Stokes and R. W. Murray, *Langmuir*, 1996, **12**, 3604.
29 C. Yee, M. Scotti, A. Ulman, H. White, M. Rafailovich and J. Sokolov, *Langmuir*, 1999, **15**, 4314.
30 M. M. Maye and C. J. Zhong, manuscript in preparation.